AIAA SciTech Forum
6-10 January 2025, Orlando, FL
AIAA SCITECH 2025 Forum

10.2514/6.2025-2598

Assessing Propellant-Optimal Guidance for Crewed Lunar Descent

Ping Lu*
San Diego State University, San Diego, CA 92182

In this paper the propellant performance advantages of modern propellant-optimal powered descent guidance in a crewed lunar mission is accessed. Two recently developed indirect-method based optimal powered descent guidance algorithm are deployed in this study, one using the conventional bang-bang thrust solution, the other utilizing an optimal constant-thrust solution. The reduction of propellant usage by employing the optimal powered descent guidance approaches is shown to be substantial and meaningful in the context of the historical data from various Apollo lunar landing missions. Moreover, it is demonstrated in this paper that propellant-optimal and Apollo-era lunar descent guidance methods can be integrated to achieve the combined strengths of propellant efficiency and autonomous operations of the new technology, and robustness and high readiness level of legacy technology. The findings in this work could serve as references to the planning and design of a forthcoming crewed lunar mission.

I. Introduction

The factors considered in the design of the powered descent trajectory of a crewed lunar mission include propellant usage, guidance margin, navigation uncertainties, landing-radar performance, terrain uncertainties, and crew visibility restrictions [1]. In this work we will focus on propellant efficiency of the powered descent guidance as other factors are more system and mission specific. Propellant consumption is at the top of this list not by accident. It was well reported that Apollo 11 Lunar Module (LM) used more propellant than anticipated because of the late divert to a safer landing location away from the originally designated site. Indeed, the final propellant margin was uncomfortably smaller than planned (see Fig. 5-12(a) in Ref. [1]). What is less publicized is that Apollo 14 LM actually had even less propellant left at touchdown (cf. the table on p. 295 of Ref. [2]). These examples highlight the critical importance of propellant efficiency in a crewed lunar descent mission.

Great strides have been made in recent years on the theory and algorithmic development in propellant-optimal powered descent guidance, including representative works based on the direct method [3–8], and those on the indirect method [9–15]. There is also a body of recent literature on propellant-optimal powered descent inside an atmosphere, which we are not including in this brief review because lunar descent is the topic here where no atmosphere is present. Thus far most demonstrations and applications of propellant-optimal powered descent guidance have been limited to landing on Mars or the Earth. When lunar landing is considered, it is usually about a short terminal part of the lunar descent [16, 17]. It should be noted that this summary of the state of the literature makes a distinction between the works aiming at guidance applications (i. e., real-time operations) and those of offline trajectory optimization, and our observation is on the former. The complete powered descent at the Moon is more than 10 times longer in the flight time and distance covered than those during powered descent at Mars. While the reasons for the lack of existing assessments of propellant-optimal guidance on a full crewed lunar descent trajectory are subject to conjectures, the significantly longer flight time undoubtedly contributes to dramatic increase in onboard computational resource requirements for direct-method based guidance approaches, and greater convergence challenges for indirect-method based approaches that typically utilize shooting methods which are prone to suffering from higher sensitivity in problems of longer duration.

The goal of NASA's Artemis Program to return astronauts to the Moon gives rise to a current interest in understanding clearly how much propellant advantage the propellant-optimal powered descent guidance may offer in a crewed lunar mission, as compared to the classical Apollo lunar descent guidance technology [18–20]. To the best knowledge of the author, this information is not presently available in the open literature. In this work we will demonstrate that the recently developed direct-method based algorithm called Guidance for Propellant-Optimal Landing of A Rocket (G-POLAR) [13] works well for the full lunar descent mission (as opposed to just a short phase). It will be shown that in a crewed

*Professor and Chair, Department of Aerospace Engineering; plu@sdsu.edu, Fellow AIAA

lunar landing mission using the same vehicle and mission data as in Apollo 11, the propellant-optimal guidance can yield a reduction of over 9% in propellant consumption when compared to the Apollo lunar descent guidance [18, 21], which is rather significant. Perhaps equally importantly, this work will demonstrate that a most recently developed constant-throttle propellant-optimal guidance algorithm in Ref. [15] (dubbed G-POLAR+) is capable of guiding a lunar crewed descent mission at just a slightly higher propellant consumption than the lowest possible value by the optimal bang-bang solution. Since the lander engine only needs to operate at a constant throttle instead of a very dynamic bang-bang profile, such an alternative allows significant reduction of the complexity of the operational requirements and even design of the engine, making such a propellant-optimal lunar descent trajectory very appealing.

Propellant optimality is only meaningful if the descent trajectory is consistent with other important operational considerations. To shape the trajectory, the Apollo 11 powered descent design splits the entire descent trajectory in 3 phases, each with a different set of target condition [19]. The same technique is not applicable to propellant-optimal trajectory because the Principle of Optimality [22] dictates that the target conditions of the phases must be on the end-to-end optimal trajectory, thus resulting in the same trajectory; the use of targeting conditions not on the end-to-end optimal trajectory will cause the overall propellant optimality to be lost. But there are other means by which the optimal trajectory can be shaped. One such approach is the so-called “pointing constraint" [5]. While the pointing constraint is originally conceived to limit the direction of the thrust vector as a way to achieve desired body attitude in a 3DOF setting, we will demonstrate that it can also shape the translational trajectory effectively if the bound of the pointing constraint is set appropriately. The unified formulation of the propellant-optimal solution in Ref. [13] produces a set of conditions valid regardless of whether the pointing constraint is active or not. A recent technique originated in Ref. [23] is modified to allow the choice of a time-varying bound of the pointing constraint as a convenient trajectory shaping parameter. This technique and the unified formulation together enable G-POLAR and G-POLAR+ to be reliable in solving the propellant-optimal powered descent problem and effective in using the pointing constraint to shape the descent trajectory close to the landing site.

Lastly, a modern propellant-optimal guidance algorithm and the propellant-efficient Apollo E-Guidance law [20] may be combined to facilitate a concept of operations where the complete powered descent is divided into a Descent Phase and a Landing Phase. We will show that the propellant-optimal guidance can competently guide the vehicle in the Descent Phase from the powered descent initiation all the way to a specified altitude above the landing site and a given descent rate. The E-Guidance law will reliably and accurately take the vehicle down to the landing site in the Landing Phase. This strategy would reap the benefit of propellant optimality of a modern algorithm like G-POLAR and enjoy the high robustness and precision of the legacy powered descent guidance for pinpoint landing.

II. Propellant-Optimal Guidance

In this section two formulations of propellant-optimal powered descent problems are reviewed, as well as the working of the guidance algorithm G-POLAR. The reader is referred to Refs. [13] and [15] for more details.

A. Standard Minimum-Propellant Powered Descent Problem

In a topocentric Cartesian coordinate frame at the landing site, the three-dimensional equations of motion during powered descent on the Moon are

$$\begin{aligned} \dot{\boldsymbol{r}} &= \boldsymbol{V}, & \boldsymbol{r}(t_0) &= \boldsymbol{r}_0 \\ \dot{\boldsymbol{V}} &= \frac{T}{m}\mathbf{1}_T + \boldsymbol{g}, & \boldsymbol{V}(t_0) &= \boldsymbol{V}_0 \\ \dot{m} &= -\frac{T}{V_e}, & m(t_0) &= m_0 \end{aligned} \tag{1}$$

where $\boldsymbol{r} = [x\ y\ z]^T$ is the position vector, $\boldsymbol{V} = [u\ v\ w]^T$ the velocity vector, and $\boldsymbol{g} = [g_x\ g_y\ g_z]^T$ is the gravitational acceleration vector which is taken to be a constant with a magnitude of $g_0 = 1.736$ m/s^2 for the Moon. $V_e > 0$ is the exhaust velocity of the engine and is considered a constant. The rocket engine thrust magnitude is T, and $\mathbf{1}_T$ is a unit vector representing the direction of the thrust vector. In this formulation of a standard optimal control problem, $\{T, \mathbf{1}_T\}$ are considered the controls in the problem, subject to the following constraints:

$$T_{min} \le T \le T_{max} \tag{2}$$

$$\mathbf{1}_T^T \mathbf{1}_T = 1 \tag{3}$$

where $T_{min} > 0$, as the engine should not be completely shut down during the powered descent. In addition, the direction of $\mathbf{1}_T$ is limited by the pointing constraint

$$\cos\Theta - \mathbf{1}_T^T \mathbf{1}_r \leq 0 \tag{4}$$

where $\mathbf{1}_r$ is the unit vector in the vertical (up) direction at the landing site, and $\Theta \geq 0$ is prescribed. The geometric interpretation of this constraint is that at any instant during the powered descent, the thrust vector must be within a pointing cone with a half apex angle of Θ. See Fig. 6 in Ref. [13].

The minimum-propellant optimal control problem involves finding the controls $\{T(t), \mathbf{1}_T(t)\}$, subject to constraints in Eqs. (2)–(4) in $[t_0, t_f]$ where $t_f > t_0$ is free, so that the trajectory of the vehicle governed by the dynamics and given initial condition in Eq. (1) satisfies the final condition

$$\begin{aligned} \boldsymbol{r}(t_f) &= \boldsymbol{r}_f^* \\ \boldsymbol{V}(t_f) &= \boldsymbol{V}_f^* \end{aligned} \tag{5}$$

where $\boldsymbol{r}_f^*$ and $\boldsymbol{V}_f^*$ are specified, and the propellant consumption represented by the following performance index is minimized

$$J = m_0 - m(t_f) \tag{6}$$

B. Unified Solution Approach

Define the primer vector in the problem

$$\boldsymbol{p}_V = -\boldsymbol{\lambda}(t - t_0) + \boldsymbol{c} \tag{7}$$

where $\boldsymbol{\lambda} \in R^3$ and $\boldsymbol{c} \in R^3$ are both constant vectors. Let

$$\mathbf{1}_{\boldsymbol{p}_V} = \boldsymbol{p}_V / \|\boldsymbol{p}_V\| \tag{8}$$

Define

$$\phi = \cos^{-1}\left(\mathbf{1}_{\boldsymbol{p}_V}^T \mathbf{1}_r\right) \tag{9}$$

Clearly ϕ is the angle between $\mathbf{1}_r$ and $\mathbf{1}_{\boldsymbol{p}_V}$. Further, define an auxiliary variable

$$\theta = \begin{cases} \phi, & \text{if } \phi \leq \Theta \\ \Theta, & \text{if } \phi > \Theta \end{cases} \tag{10}$$

The first condition in Eq. (10) is when the pointing constraint is inactive, and the second signifies when the pointing constraint is active. Then the optimal thrust direction at any instant is given by

$$\mathbf{1}_T^* = \frac{\sin(\phi - \theta)}{\sin\phi}\mathbf{1}_r + \frac{\sin\theta}{\sin\phi}\mathbf{1}_{\boldsymbol{p}_V} \tag{11}$$

The optimal thrust magnitude, on the other hand, is determined by the following condition

$$T^* = \begin{cases} T_{max}, & S(t) > 0 \\ T_{min}, & S(t) < 0 \end{cases} \tag{12}$$

where with $p_V = \|\boldsymbol{p}_V\|$, the switching function $S(t)$ is given by

$$S(t) = \frac{1}{m}\left[\frac{\sin(\phi - \theta)}{\tan\phi} + \frac{\sin\theta}{\sin\phi}\right] p_V - \frac{p_m}{V_e} \tag{13}$$

where the mass costate p_m is governed by the following differential equation and boundary condition

$$\dot{p}_m = \frac{T^*}{m^2}\left[\frac{\sin(\phi - \theta)}{\tan\phi} + \frac{\sin\theta}{\sin\phi}\right] p_V, \quad p_m(t_f) = 1 \tag{14}$$

The theoretically optimal solution for the thrust magnitude is "bang-bang" as shown in Eq. (12). The bang-bang solution may actually cause operational concerns in a lander. For instance, see some of the reasons in Ref. [17]. In G-POLAR, the commanded thrust magnitude is given by a close continuous approximation to the bang-bang solution in Eq. (12):

$$T^*(t) = \frac{1}{2}\left(T_{max} + T_{min}\right) + \frac{1}{2}\left(T_{max} - T_{min}\right)\tanh\left[\frac{S(t)}{1-\varepsilon}\right], \quad 0 < \varepsilon < 1 \tag{15}$$

where ε is a parameter. The closer ε is to unity, the sharper the switches of T^* between T_{max} and T_{min} are. Our experience has been that the propellant consumption penalty of using the smoothed thrust in Eq. (15) as compared to the theoretical optimum is practically negligible.

Remarks:

1) While in Ref. [13] Θ is treated as a constant, the theoretical optimality and all the equations remain applicable when Θ is an explicitly defined function of time.
2) The above equations are valid regardless of whether the pointing constraint in Eq. (4) is active or not. There is no need for the algorithm to design branches to handle the cases differently. This proves to be a major benefit for robust convergence of G-POLAR.
3) An active pointing constraint (when $\phi - \theta \neq 0$ by Eq. (10)) not only changes the the direction of the optimal thrust vector by causing $\mathbf{1}_T^*$ to have a component along $\mathbf{1}_r$ (see Eq. (11)), but also affects the optimal engine throttle (see the presence of $\sin(\phi - \theta)$ in Eq. (13) and Eq. (14)). The latter is not intuitive if not revealed by Eqs. (13) and (14).
4) For the specifics of the numerical solution process, see Ref. [13].

C. Constant-Throttle Propellant-Optimal Powered Descent

The solution to the standard propellant-optimal powered descent problem requires that thrust magnitude have a bang-bang profile, switching instantaneously between T_{min} and T_{max} (see Ref. [13] for instance for a theoretical discussion). In practice flying such a bang-bang thrust profile may face a number of difficulties and challenges [15]. To circumvent these issues, an alternative of parameterized-thrust propellant-optimal powered descent solution is proposed in Ref. [15]. In this approach, the user prescribes a parameterized continuous function of time for the engine thrust profile in a propellant-optimal powered descent problem that has all the elements of the problem in the subsection II.A. The solution finds the optimal thrust direction, time of flight, and the parameters that completely and uniquely define the thrust function, to minimize the propellant consumption. Such a problem still provides a propellant-optimal solution, just under the restriction that the thrust has the prescribed functional form. It is shown in Ref. [15] that when the thrust is parameterized by a zeroth-order polynomial of time, a constant, the propellant consumption of the optimal constant-throttle solution is only $1 \sim 2\%$ higher than that of the optimal bang-bang solution; if the thrust is represented by a linear function of time, the optimal linear-throttle solution would recover most of the already small propellant performance loss by the constant-throttle solution. Given its great simplicity, respectable propellant performance, and guidance robustness, just the constant-throttle propellant-optimal formulation and solution approach are reviewed below.

The problem formulation is the same as in Section II.A, except that the engine thrust T is no longer treated as a control, but a user-prescribed function of time with a design parameter vector $\boldsymbol{d} \in R^k$, $k \geq 1$:

$$T = f_T(t, \boldsymbol{d}) \tag{16}$$

where f_T has a specified functional form, and the optimal value of the to-be-determined constant $\boldsymbol{d}$ is part of the solution to the problem. In particular, we consider the case where

$$T = T_c \tag{17}$$

where T_c is a constant thrust that satisfies the constraints in Eq. (2). Therefore in this case $d = T_c$. A consequence of a T as a prescribed function of time is that the mass of the vehicle is not a state variable anymore, but an explicit function of time and the parameter T_c

$$m(t, T_c) = m_0 - \frac{T_c}{V_e}(t - t_0) \tag{18}$$

The unified solution approach in Section II.B and all the equations remain applicable, except for Eqs. (12) – (15) which are no longer needed, as T is given by Eq. (17) now. The additional condition required to determine the optimal value of T_c is [24]

$$\int_{t_0}^{t_f} \frac{\partial H}{\partial T_c} dt = 0 \tag{19}$$

where H is the Hamiltonian of the problem, and the explicit dependence of H on T_c is through $T = T_c$ and $m(t, T_c)$ in Eq. (18). It can be shown that the condition in Eq. (19) may be expanded to (see Ref. [15])

$$\int_{t_0}^{t_f} \left\{ \frac{m_0}{m^2(t,T_c)} \left[\frac{\sin(\phi-\theta)}{\tan\phi} + \left(\frac{\sin\theta}{\sin\phi} \right) \| -\boldsymbol{\lambda}(t-t_0) + \boldsymbol{c} \| \right] - \frac{1}{V_e} \right\} dt = 0 \tag{20}$$

where the optimal thrust direction in Eq. (11) has been used. Define an augmented state y_1 by the solution of the system

$$\dot{y}_1 = \frac{m_0}{m^2(t,T_c)} \left[\frac{\sin(\phi-\theta)}{\tan\phi} + \left(\frac{\sin\theta}{\sin\phi} \right) \| -\boldsymbol{\lambda}(t-t_0) + \boldsymbol{c} \| \right] - \frac{1}{V_e}, \quad y_1(t_0) = 0 \tag{21}$$

Then the integral condition in Eq. (20) is equivalent to a more conventional terminal constraint

$$y_1(t_f) = 0 \tag{22}$$

Much of the G-POLAR guidance algorithm remains applicable to the constant-throttle propellant-optimal powered descent problem. If anything, the algorithm is simpler because there is no need to deal with the technicality associated with the switches of the thrust magnitude and numerical issues caused by the bang-bang discontinuity. The one consequential difference is that the constraint $p_m(t_f) = 1$ (cf. Eq. (14)) is now replaced by the terminal condition in Eq. (22). The algorithm that solves this constant-throttle problem is dubbed G-POLAR+ [15].

The optimal constant-throttle guidance is a very appealing alternative to the long-held bang-bang propellant-optimal approach. At a comparable propellant performance, not only all the potential difficulties associated with flying bang-bang throttle trajectory are avoided, but the guidance is significantly more robust because the constant throttle is typically far from being saturated at the maximum (or minimum) bound. Furthermore, not requiring the engine of the lander to perform rapid throttle modulation could conceivably reduce the complexity of the engine. See Ref. [15] for more discussion.

It should be noted in Ref. [15], the optimal linear-throttle solution is also considered. And it is shown in Ref. [15] the optimal linear-throttle solution yields practically the same propellant performance as the bang-bang throttle solution. But in this paper we will just use the optimal constant-throttle solution because of its extreme simplicity.

III. Trajectory Shaping by Time-Varying Pointing Constraint

The pointing constraint in Eq. (4) is originally conceived to limit the body attitude of the lander which is represented by the thrust vector direction. As it turns out, this constraint can have a strong effect on shaping the powered descent trajectory, depending on what the bound Θ is. The choice of Θ must balance competing considerations: too small a Θ will severely restrict the trajectory to the point where no solution may even exist to the problem; too large a Θ may not have the desirable effect. Indeed, a constant Θ may not work well in most cases. In Ref. [23] a time-varying Θ is proposed, and the technique appears to offer a good way to balance the requirement of relatively unrestricted pointing of the thrust vector early in the descent and limiting the thrust direction close to the vertical direction near the end. We will first discuss this technique and provide a modified alternative to better serve our purposes.

Use similar notation as in Ref. [23] and choose two positive constant $\dot{\Theta}_{max} > 0$ and $\ddot{\Theta}_{max} > 0$. Define

$$\theta_R = \dot{\Theta}_{max} t_{go} \tag{23}$$

$$\theta_A = \frac{1}{2} \ddot{\Theta}_{max} t_{go}^2 \tag{24}$$

where t_{go} is the current time-to-go. Assume that $\dot{\Theta}_{max}$ is in deg/s and $\ddot{\Theta}_{max}$ in deg/s^2. Define

$$t_{go_1} = \frac{90}{\dot{\Theta}_{max}}, \quad t_{go_2} = \frac{\dot{\Theta}_{max}}{\ddot{\Theta}_{max}} \tag{25}$$

where t_{go_2} is the instant when $\dot{\theta}_A = \dot{\Theta}_{max}$. The choice of Θ in degrees proposed in Ref. [23] is

$$\Theta(t) = \begin{cases} 90, & t_{go} \geq t_{go_1} \\ \theta_R, & t_{go_2} < t_{go} < t_{go_1} \\ \theta_A, & t_{go} \leq t_{go_2} \end{cases} \tag{26}$$

The rationale for the sequence in Eq. (26) is to maintain $\dot{\Theta} \le \dot{\Theta}_{max}$, and $\ddot{\Theta} \le \ddot{\Theta}_{max}$ during the descent, because Θ may be regarded as the pitch-over angle when the pointing constraint is active. While it is not discussed in Ref. [23], it can be shown that for the order of sequence in Eq. (26) to hold (namely, $t_{go_1} > t_{go_2}$), the following condition needs to be met

$$\frac{\dot{\Theta}_{max}^2}{\ddot{\Theta}_{max}} \le 90 \tag{27}$$

Moreover, when switching from θ_R to θ_A at t_{go_2}, there is a discontinuity in Θ

$$\Delta\Theta = \theta_R(t_{go_2}) - \theta_A(t_{go_2}) = 0.5\frac{\dot{\Theta}_{max}^2}{\ddot{\Theta}_{max}} \neq 0 \tag{28}$$

Through extensive experiments we have determined that θ_A plays the predominant role, and the benefit of including θ_R in the formulation of $\Theta(t)$ is negligible, not to mention using it in Eq. (26) necessitates the restrictive condition in Eq. (27) and $\Theta(t_{go_2})$ suffers from the discontinuity in Eq. (28) which cannot be physically realized. Therefore we opt to modify the formation of Θ by a simpler, universally applicable, and continuous alternative

$$\Theta(t) = \begin{cases} 180, & \theta_A \ge 180 \\ \theta_A = \frac{1}{2}\ddot{\Theta}_{max} t_{go}^2, & \theta_A < 180 \end{cases} \tag{29}$$

Discussion:

1) The $\Theta(t)$ in Eq. (29) is not capped at 90 deg as in Eq. (26) but at 180 deg, because for lunar descent the vehicle initially is far from the landing site, and the optimal thrust vector initially may need to take up an angle of more than 90 degrees with respect to $\mathbf{1}_r$ which is located at the landing site at a long downrange over the curved lunar surface from where the vehicle is.
2) Since $\Theta \to 0$ as $t_{go} \to 0$, the pointing constraint is necessarily active for any $\ddot{\Theta}_{max} > 0$ as t_{go} gets smaller. Furthermore, the angle between $\mathbf{1}_T$ and $\mathbf{1}_r$ will necessarily achieve the conditions of $\theta \to 0$ and $\dot{\theta} \to 0$ just like Θ will. These conditions ensure that the vehicle will land vertically with a zero tilt rate, if the thrust direction is fixed with the longitudinal body axis of the vehicle.
3) While $\ddot{\Theta}_{max}$ can have a physical meaning of pitch-over acceleration when the pointing constraint is active, it is not helpful to fixate on the interpretation that it has to be chosen to represent the maximum pitch-over acceleration the vehicle may have. Rather, it would be much more productive to view $\ddot{\Theta}_{max}$ as a trajectory shaping parameter, and choose its value accordingly. Indeed, as will be demonstrated in Section VI later, an appropriate value of $\ddot{\Theta}_{max}$ leading to a desirable trajectory can be significantly smaller than typical maximum angular acceleration a vehicle may produce.
4) The discussion in this section applies to both constant-throttle and bang-bang propellant-optimal powered descent problems.

IV. Apollo Lunar Descent Guidance and Its Modern-day Family

The Apollo-era powered descent guidance designs are represented by the Apollo lunar descent guidance law [18] that was flown in the Apollo missions, and the E-Guidance law [20] that was not flown, but later was found to be the solution to an optimal powered descent problem with a quadratic performance index on the engine thrust [25] (which is different from propellant optimal). More recently, a large two-parameter family of Fractional-Polynomial Powered Descent Guidance (FP^{2}DG) laws are discovered that include the Apollo lunar descent guidance and E-Guidance laws as two members of the family [26]. The FP^{2}DG guidance laws are defined on the thrust acceleration vector $\boldsymbol{a}_T = T\mathbf{1}_T/m$ by

$$\begin{aligned} \boldsymbol{a}_T &= \gamma\left[\frac{k_r}{2(\gamma+2)} - 1\right]\boldsymbol{a}_{T_f}^* + \left[\frac{\gamma k_r}{2(\gamma+2)} - \gamma - 1\right]\boldsymbol{g} \\ &+ \frac{(\gamma+1)}{t_{go}}\left(1 - \frac{k_r}{\gamma+2}\right)(\boldsymbol{V}_f^* - \boldsymbol{V}) + \frac{k_r}{t_{go}^2}\left(\boldsymbol{r}_f^* - \boldsymbol{r} - \boldsymbol{V}t_{go}\right) \end{aligned} \tag{30}$$

where the guidance law parameters γ and k_r can be chosen arbitrarily provided that $\gamma \ge 0$ and $k_r \ge 2(\gamma+2)$. The vector $\boldsymbol{a}_{T_f}^*$ is the final thrust acceleration (magnitude and direction) the user specifies for the vehicle. The reader is referred to Ref. [26] for the detailed interpretations of the parameters γ and k_r and the FP^{2}DG laws.

Specifically, when $\gamma = 1$, the FP^{2}DG laws reduce to the Augmented Apollo Powered Descent Guidance (A^{2}PDG) law [27]:

$$\boldsymbol{a}_T = \left(\frac{k_r}{6} - 1\right)\boldsymbol{a}^*_{T_f} + \left(\frac{k_r}{6} - 2\right)\boldsymbol{g} + \frac{2}{t_{go}}\left(1 - \frac{k_r}{3}\right)(\boldsymbol{V}^*_f - \boldsymbol{V}) + \frac{k_r}{t^2_{go}}\left(\boldsymbol{r}^*_f - \boldsymbol{r} - \boldsymbol{V}t_{go}\right) \tag{31}$$

When $k_r = 6$, the A^{2}PDG law becomes the E-Guidance law [20]

$$\boldsymbol{a}_T = -\boldsymbol{g} - \frac{2}{t_{go}}(\boldsymbol{V}^*_f - \boldsymbol{V}) + \frac{6}{t^2_{go}}\left(\boldsymbol{r}^*_f - \boldsymbol{r} - \boldsymbol{V}t_{go}\right) \tag{32}$$

When $k_r = 12$, the A^{2}PDG law transforms into the Apollo lunar descent guidance law [18]

$$\boldsymbol{a}_T = \boldsymbol{a}^*_{T_f} - \frac{6}{t_{go}}(\boldsymbol{V}^*_f - \boldsymbol{V}) + \frac{12}{t^2_{go}}\left(\boldsymbol{r}^*_f - \boldsymbol{r} - \boldsymbol{V}t_{go}\right) \tag{33}$$

It can be shown that the E-Guidance law will terminate with a final thrust acceleration of $\boldsymbol{a}_T(t_f) = -2\boldsymbol{g}$, and the Apollo lunar guidance law will end with $\boldsymbol{a}_T(t_f) = \boldsymbol{a}^*_{T_f}$ [26].

The optimal t_{go} for the E-Guidance in the quadratic optimal control problem can be calculated analytically, as a function of the current position and velocity vectors $\boldsymbol{r}$ and $\boldsymbol{V}$ [25]. Once the initial t_{go} is assigned (with the optimal value or otherwise), the E-guidance law in Eq. (32) has no free parameter to adjust for trajectory shaping. The user must determine an appropriate initial value of t_{go} for the Apollo lunar descent guidance law in Eq. (33), and can choose $\boldsymbol{a}^*_{T_f}$ for trajectory shaping. The FP^{2}DG laws in Eq. (30), on the other hand, can use both γ and k_r, as well as $\boldsymbol{a}^*_{T_f}$ (as long as $k_r > (2(\gamma + 2))$, to affect the trajectory. A demonstration of using the FP^{2}DG guidance laws and γ and k_r to shape the trajectory in crewed lunar landing is presented in Ref. [28].

It should be noted that unlike in the propellant optimal solution, the upper and lower bounds on the thrust in Eq. (2) are not considered in the design of FP^{2}DG laws and any of the Apollo-era guidance laws. The pointing constraint in Eq. (4) is also not explicitly considered. But the choice of $\boldsymbol{a}^*_{T_f}$ can be leveraged to control the pointing direction in the final part of the trajectory provided $k_r > (2(\gamma + 2)$.

V. Combining Propellant-Optimal Guidance and E-Guidance

It will be demonstrated in the next section that G-POLAR and G-POLAR+ work well in guiding a crewed lunar descent and landing mission from the powered descent initiation (PDI) to touchdown in a single phase. But operationally, it may be more desirable to have a clear final vertical landing phase, just like in the trajectory design of the Apollo 11 LM descent [21]. Such a phase would give the crew the opportunity to continue monitoring the lander trajectory and the option of manual control during the final landing. The descent rate is low in such a phase and the propellant optimality is not essential as long as the guidance is still propellant efficient. But accurate attainment of the touchdown condition is important and the guidance should be highly robust and accurate in this phase to accommodate any expected dispersions at the start of the final phase.

Toward this goal, the powered descent trajectory from the PDI to touchdown may be divided into a main Descent Phase and a final Landing Phase. The transition condition between the two phases will be defined in trajectory design. In Apollo 11 descent trajectory design, this is known as the ”low gate" [21]. This condition can be, for instance, defined by a specified altitude above the landing site and a prescribed descent rate at the point. The Descent Phase is from the PDI to this transition condition, guided by G-POLAR or G-POLAR+ for propellant optimality. The target position vector $\boldsymbol{r}^*_f$ for G-POLAR/G-POLAR+ in Eq. (5) now will represent the point above the landing site at the given altitude, and $\boldsymbol{V}^*_f$ the specified descent velocity at that point.

The Landing Phase will then be guided by the E-Guidance law in Eq. (32) where the target condition represents the specified touchdown condition. The E-Guidance law is chosen because of two features associated with it: (a) E-Guidance law is theoretically propellant efficient (as it tends to keep the average thrust low); (b) the optimal time-to-go for the E-Guidance law can be analytically computed, based on the current trajectory state. As such the guidance system requires no user-supplied input for t_{go}.

This guidance strategy would draw the best strengths of a modern guidance capability and a legacy technology, allowing propellant optimality in the Descent Phase, and highly robust pinpoint landing precision even in the Landing Phase.

VI. Assessment with a Crewed Landing Mission at Lunar South Pole

A. Mission and Vehicle Model

The vehicle data of the Apollo 11 Lunar Module (LM) [29] are used in the numerical results in this section. The landing site is the South Pole of the Moon. The PDI is assumed at the pericynthion of the descent orbit, as is in the Apollo 11 mission. The PDI condition is essentially the same as that for Apollo 11 LM [1, 30], except for the modifications necessary for a landing at the South Pole. The PDI condition and vehicle data are summarized in Table. 1.

Table 1 PDI condition at pericynthion, landing site, and vehicle data

Parameter	Value
Altitude (km)	15.24
Longitude (deg)	41.85
Latitude (deg)	-71.6
Inertial velocity (m/s)	1,698.3
Inertial flight path angle (deg)	0.0
Landing site longitude (deg)	41.85
Landing site latitude (deg)	-90.0
Downrange to landing site (km)	559.41
Crossrange to landing site (km)	0.48
Total vehicle mass (kg)	15,103.0
Propellant mass (kg)	8,248
Maximum engine thrust (N)	45,000
Minimum engine thrust (N)	4,500
Engine exhaust velocity (m/s)	3,048.8

The touchdown condition at the landing site is defined by a vertical velocity of -1.0 m/s with zero horizontal velocity at a planetodetic altitude of 0.0 m. All the numerical results presented in this section are from closed-loop 3DOF simulations, with a guidance frequency of 5 HZ. To focus on guidance performance, perfect navigation is assumed in the simulations. For the calculation of planetodetic altitude, the Moon is modeled as an ellipsoid. The gravitational acceleration vector used in the simulations of the vehicle's trajectory is from a spherical harmonic model including the J_2 terms (in contrast to the constant gravity used in the powered descent guidance solutions).

To establish a baseline, the nominal trajectories under the optimal bang-bang guidance by G-POLAR and optimal constant-throttle guidance by G-POLAR+ are obtained where the pointing constraint in Eq. (4) is not yet imposed. Table. 2 lists the propellant consumption and time of flight for each of the two trajectories. It is seen that the propellant consumption by the constant-throttle guidance is only 96 kg more than the bang-bang solution, or a mere 1.5% increase. Figure 1 shows the comparison the two trajectories in the North-Up-East topocentric frame at the landing site, and the profiles of planeto-detic altitude versus ground range. The two trajectories are very close to each other. The engine throttle profiles are depicted in Fig. nominal throttle. Notice that even though G-POLAR+ generate the guidance command in each guidance cycle based on a constant-throttle solution, the differences between the closed-loop simulation and the simplified model G-POLAR+ used to generate the guidance command cause a slow and gradual increase of the actual throttle profile (the blue curve in the figure). This is typical phenomenon in closed-loop guidance simulations.

Table 2 Propellant consumption under optimal bang-bang and linear-throttle guidance approaches

	bang-bang	constant-throttle
Propellant usage (kg)	6,703	6,799
Time of flight (s)	562.1	606.3

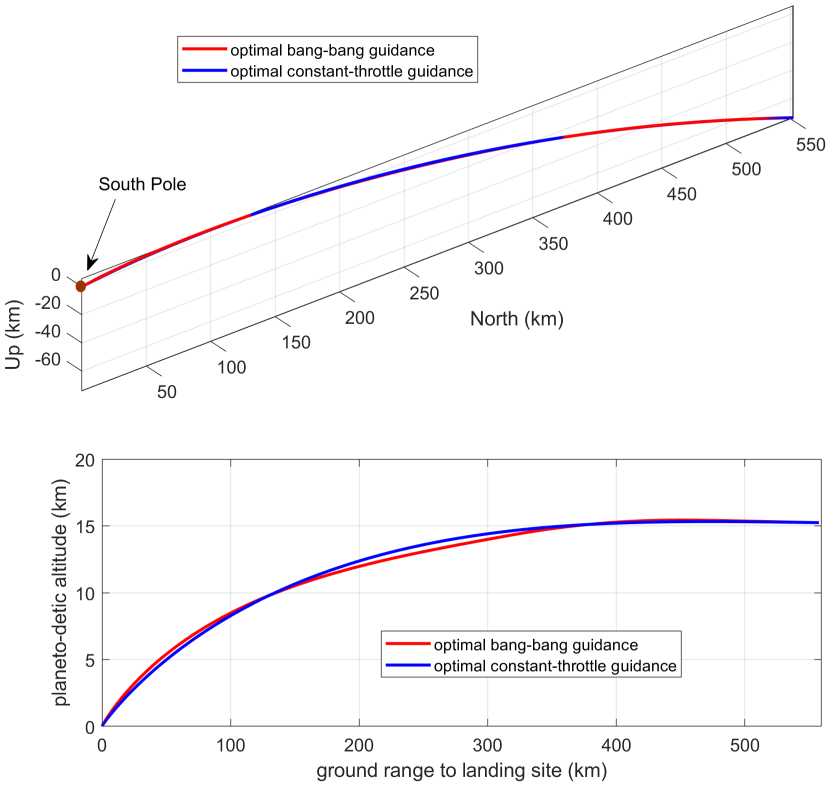

Fig. 1 Nominal optimal bang-bang and linear-throttle powered descent trajectories, without enforcing pointing constraint in Eq. (4): top – trajectories in a topocentric frame at South Pole; bottom – planetodetic altitude vs ground range

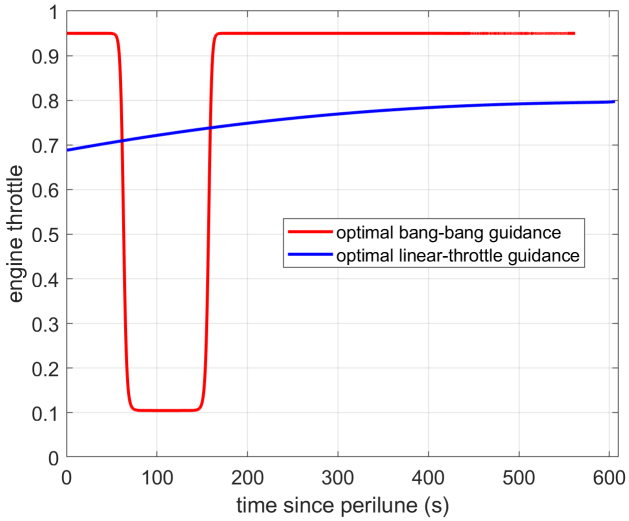

Fig. 2 Nominal optimal bang-bang and linear-throttle engine throttle profiles, without pointing constraint in Eq. (4)

B. Trajectory Shaping and Propellant Consumption by Fuel-Optimal Guidance

Given the similarity in the nominal trajectories under the optimal bang-bang and constant-throttle guidance, in this section only the bang-bang guidance by G-POLAR is used in examining the influence of the pointing constraint. In the G-POLAR solution generation process, a 5% margin is reserved on the maximum and minimum thrust levels for closed-loop tracking later in the trajectory. See Ref. [13] for more on the topic of tracking. To demonstrate the effect of shaping the trajectory by the pointing constraint in Eq. (4) with the bound Θ defined by Eq. (29), several different values of $\ddot{\Theta}_{max}$ are used, as well as the unconstrained case (where the pointing constraint is not imposed).

Figure 3 shows the altitude profiles versus ground range to landing site in these cases. The zoom-in insert on the last portion of the trajectories vividly illustrates the clear and predictable effects of $\ddot{\Theta}_{max}$ in affecting the trajectories, particularly near the end. The unconstrained case has a very shallow trajectory during the last segment. The presence of the pointing constraint notably turns the trajectory more vertical before touchdown, signifying the fact that the pointing constraint will become active when the time-to-go is below a certain threshold. The smaller $\ddot{\Theta}_{max}$ is, the more pronounced this nearly vertical terminal segment becomes.

The thrust pointing angles along the these trajectories are depicted in Fig. 4. The unconstrained case has a final pointing angle of about 60 deg, indicating a substantial horizontal component of the thrust vector is still being used near the end of the descent, not to mention that the vehicle attitude is nowhere close to being vertical. When the pointing constraint is imposed, there is a quick pitch-over in the last moment to achieve a nearly zero pointing angle. Note that from Fig. 4 one can see clearly the rationale for allowing 180 deg in Θ in Eq. (29) as opposed to capping it at 90 deg: in the initial phase of the powered descent the vehicle's thrust pointing angle with respect to the local vertical at the landing site can be greater than 90 deg in lunar descent, and it would be unnecessarily restrictive to limit it below 90 deg.

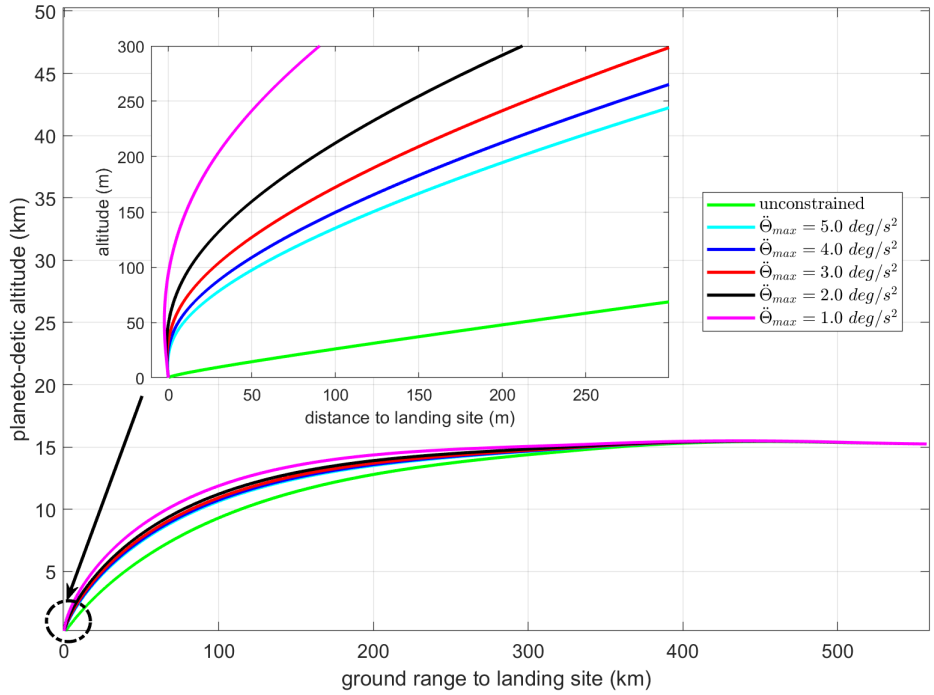

Fig. 3 Trajectory shaping effect of the pointing constraint Eq. (4) as seen in altitude-vs-ground range profiles for different values of values of $\ddot{\Theta}_{max}$

The engine throttle histories along the trajectories are given in Fig. 5. The presence of the pointing constraint not only has a major influence on the thrust direction as represented by the pointing angle in Fig. 4, but also affects the engine throttle by shifting the switching times between the upper and lower bounds, as is evident in Fig. 5.

The propellant consumption under the guidance by G-POLAR in each case is tabulated in Table 3. As expected, the least propellant consumption is achieved by the unconstrained case (which may be regarded as the case where

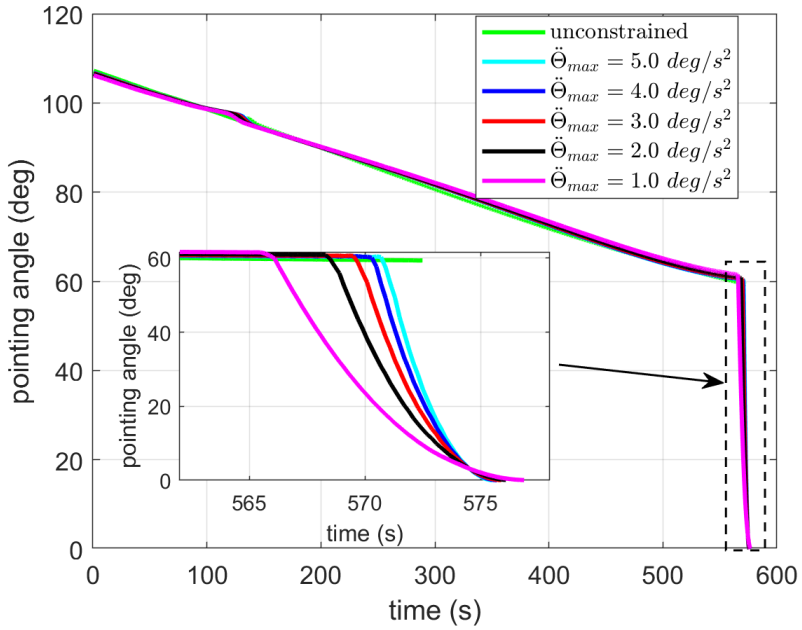

Fig. 4 Thrust pointing angle profiles of the vehicle (measured with respect to the vertical direction at the landing site) along the G-POLAR guided trajectories

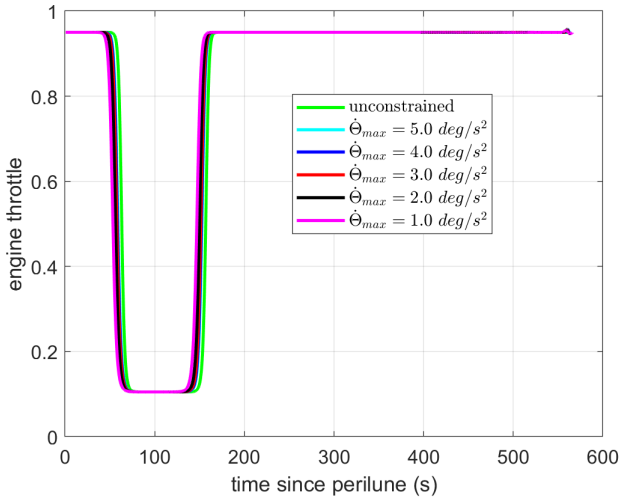

Fig. 5 Engine throttle profiles along the G-POLAR guided trajectories

$\ddot{\Theta}_{max} = +\infty$), and the smaller $\ddot{\Theta}_{max}$ is, the higher the propellant consumption is. But what is surprising is the discovery that the propellant penalty with the enforcement of the pointing constraint is very mild in lunar descent, ranging from 0.4% to 0.8% in the cases tested. This is likely because the long flight time in a crewed lunar descent (about 580 seconds under G-POLAR) allows the optimal solution to compensate for/lessen the propellant penalty by the anticipated, vigorous but short pitch-over maneuver at the end (cf. Fig. 4). We can confirm from our own study that the propellant penalty by the pointing constraint in a human-scale Mars powered descent mission (which would last less than one-tenth of the time of flight in a lunar descent) would be one-order of magnitude higher than seen here.

It should be mentioned that for the lunar descent trajectory covering more than 550 km in ground range, the fidelity of the open-loop optimal solution based on the constant gravity model in Eq. (1) is not high. For instance, the very

Table 3 Propellant consumption by G-POLAR

$\ddot{\Theta}_{max}$ (deg/s^2)	Propellant usage (kg)
unconstrained	6,703
5.0	6,727
4.0	6,729
3.0	6,735
2.0	6,741
1.0	6,757

first solution without the pointing constraint generated by G-POLAR at the PDI predicts a final propellant usage of 6,405 kg which is exactly the same as in the open-loop solution found by an independent pseudospectral optimal control software [31]. This is more than 300 kg less than the 6,727 kg consumed in closed-loop simulation as given in Table 3, a manifestation of the difference between the simplified dynamics model in Eq. (1) and the dynamics with a central gravitational field in the simulations. Incidentally, the pseudospectral optimal control software in Ref. [31] would find a propellant usage of 6,671 kg in the open-loop solution in a Newtonian gravity field for the same problem. Still closed-loop guidance always ensures high accuracy in meeting the touchdown condition. The prediction of the propellant consumption in the optimal solution will become more accurate as the trajectory gets shorter.

C. Applying Apollo Lunar Descent Guidance

For the PDI condition given in Table 1, the optimal initial time-to-go for the E-Guidance law in Eq. [20] is found to be 762.3 seconds [25]. For the Apollo lunar descent guidance law in Eq. (33), the initial t_{go} will need be determined to balance the propellant consumption and throttle margin (so as not to saturate the throttle at the upper and lower bounds). There is no known theoretical techniques to do this, and trials by closed-loop simulations typically help finding an appropriate value effectively. In this case the value of 762.3 seconds appears to work well for the Apollo lunar descent guidance law (which is not always the case). And this value is also close to the reported burn time of 756 seconds of the powered descent of the Apollo LM [30]. Therefore the same initial $t_{go} = 762.3$ sec is used for both E-Guidance and Apollo lunar descent guidance laws in this section.

For the Apollo lunar descent guidance law, the targeted final thrust acceleration vector $\boldsymbol{a}^*_{T_f}$ also needs to be chosen. The direction of $\boldsymbol{a}^*_{T_f}$ is chosen to control the final thrust direction. As shown in Ref. [26], the E-Guidance law will produce a final thrust acceleration of $-2\boldsymbol{g}$ (where $\boldsymbol{g}$ is the gravitational acceleration vector of the Moon and has a magnitude of 1.62 m/s^2). Thus for the first comparison, $\boldsymbol{a}^*_{T_f} = -2\boldsymbol{g}$ is chosen for the Apollo lunar descent guidance law.

The trajectories under the E-Guidance and Apollo lunar descent guidance laws with $\boldsymbol{a}^*_{T_f} = -2\boldsymbol{g}$ for the same mission can be seen in Fig. 6. Both trajectories have a loft, especially under the Apollo lunar descent guidance law: the altitude would rise to over 35 km (from an initial altitude of 15 km) before descending down to the landing site. This very pronounced counter-intuitive characteristic cannot be operationally desirable. The Apollo 11 descent trajectory design addressed this behavior by dividing the descent trajectory into 3 phases and using appropriate targeting condition for each phase [18, 19] It turns out that $\boldsymbol{a}^*_{T_f}$ in the Apollo lunar descent guidance law is also a very effective "knob" that can be adjusted to eliminate the trajectory loft. Plotted in Fig. 6 is another trajectory that is guided by the Apollo lunar descent guidance law with an $\boldsymbol{a}^*_{T_f} = -(2/1.62)\boldsymbol{g} = -1.235\boldsymbol{g}$ (which has a magnitude of 2.0 m/s^2). This trajectory is completely void of the undesirable loft. The E-Guidance law does not have any such knob to turn once the targeting condition and initial t_{go} have been defined.

The engine throttle profiles of the 3 trajectories are shown in Fig. 7. The pointing angle profiles are given in Fig. 8. When the direction of $\boldsymbol{a}^*_{T_f}$ is chosen in the vertical direction, the final pointing angle under the Apollo lunar descent guidance law is ensured to be zero, a very nice feature of the guidance law. The variations of the pointing angle (consequently, the direction of the thrust vector) under the Apollo lunar descent guidance law can be strongly nonlinear though, as is evident in Fig. 8.

The propellant consumption by each of the 3 trajectories in Fig. 6 is listed in Table 4. These numbers are notably higher than the propellant consumption by G-POLAR in Table 3, with the largest difference at **685** kg, a saving of 9.3%

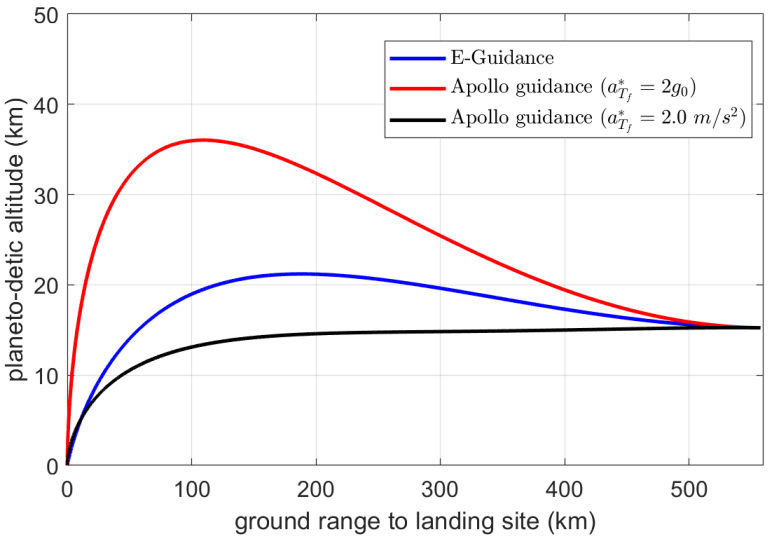

Fig. 6 Descent trajectories guided by Apollo-era guidance laws

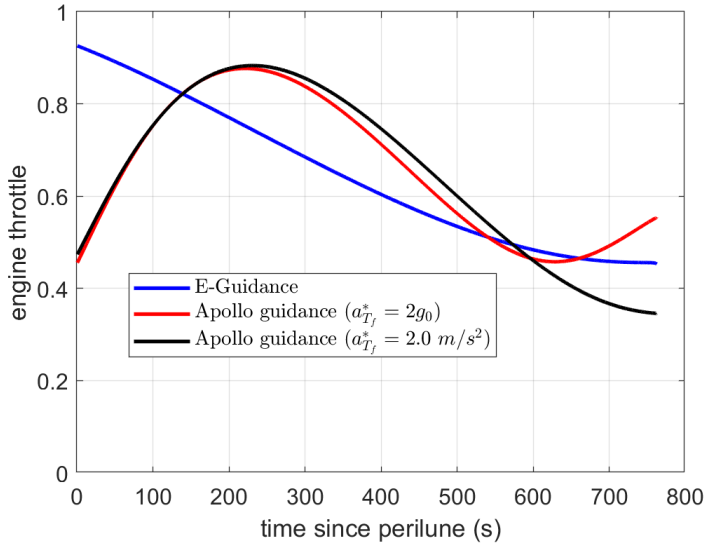

Fig. 7 Engine throttle profiles by Apollo-era guidance laws

over the propellant usage by Apollo lunar descent guidance, and equal to 8.3% of the total propellant in the Apollo 11 descent stage as listed in Table 1.

Table 4 Propellant consumption by Apollo guidance laws

Guidance law	Propellant usage (kg)
E-Guidance, Eq. (32)	7,232
Apollo lunar descent guidance, Eq. (33) with $\boldsymbol{a}^*_{T_f} = 2\boldsymbol{g}$ ($\|\boldsymbol{a}^*_{T_f}\| = 3.244$ m/s^2)	7,413
Apollo lunar descent guidance, Eq. (33) with $\boldsymbol{a}^*_{T_f} = -1.236\boldsymbol{g}$ ($\|\boldsymbol{a}^*_{T_f}\| = 2.0$ m/s^2)	7,324

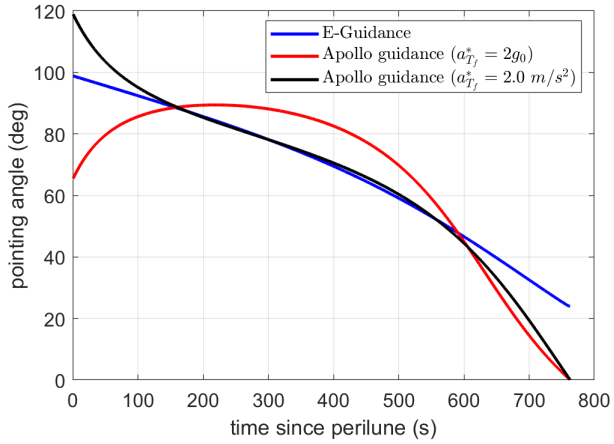

Fig. 8 Thrust pointing angle profiles by Apollo-era guidance laws

It should be stressed that the propellant performance of the Apollo-era powered descent guidance laws and their recently discovered family, the FP^{2}DG laws, are strongly influenced by the choice of the initial value of t_{go}. The selection of $\boldsymbol{a}^*_{T_f}$ has some impact on propellant usage as well. The FP^{2}DG laws have two additional free parameters γ and k_r that may be adjusted. Hence the propellant performance of the Apollo lunar descent guidance law and FP^{2}DG laws in general may be further improved still by using a better set of these parameters. But the choices of these parameters will also affect the shape of the trajectory (as seen in this section). And more importantly, there is not an existing systematic way to determine the values of these parameters for meeting the sometimes competing demands for propellant efficiency and trajectory shaping. In case of a contingency such as significant off-nominal condition and divert, determining these guidance parameters onboard to ensure a successful and still fuel-efficient trajectory remains challenging. In contrast, a fully automated propellant-optimal guidance algorithm would be able to generate all the necessary information and guidance commands based on the actual condition and updated landing site coordinates.

D. Descent and Landing Phase Guidance

Now we divide the entire powered descent trajectory into the Descent Phase and Landing Phase. The Descent phase starts at PDI and ends above the landing site at a specified altitude and descent rate. The Landing Phase follows with a vertical descent and ends at touchdown. G-POLAR will guide the lander in the Descent Phase, and E-Guidance law in the Landing Phase. The initial time-to-go for the E-Guidance law is obtained analytically [25] based on the condition at the start of the Landing Phase. For the numerical results in this subsection, the phase transition condition is somewhat arbitrarily set to be an altitude of 100 m above the landing site and a descent rate of 5 m/s. This condition is close but not identical to the low-gate condition for Apollo 11 LM descent [21]. The guidance strategy described here allows the user to choose the transition condition at will and no other information is required from the user.

Figure 9 shows several descent trajectories near the landing site where the Landing Phase can be seen clearly. Three different values of $\ddot{\Theta}_{max}$ are used in the pointing constraint for G-POLAR as well as the unconstrained case (without the pointing constraint). In comparison with Fig. 3, the presence of the Landing Phase creates a consistent landing condition, regardless of the differences in the trajectory in the Descent Phase.

To gain a comparison of the trajectories in the Descent Phase guided by G-POLAR and Apollo lunar descent guidance, the two full trajectories are plotted in Fig. 10, where $\ddot{\Theta}_{max}$ = 3.0 deg/s^2 is used in G-POLAR. The difference is very visible in the second half of the Descent Phase. Still, the insert in Fig. 10 shows that the trajectory in the Landing Phase in both cases is practically the same. The trajectory difference in the Descent Phase attributes to different propellant usages. Table 5 provides the breakdown of the propellant consumption in the Descent and Landing Phases, and the overall propellant usage, under the two guidance combinations. With the same Landing Phase, G-POLAR offers a saving of **593** kg in propellant consumption as compared to Apollo lunar descent guidance. This is a saving of 8.1%, and amounts to 7.8% of the total usable propellant in the Apollo 11 descent stage (see Table 1); at a 30% engine throttle during the Landing Phase as can be seen in Fig. 11, this amount of propellant would give the lander more than 2 minutes

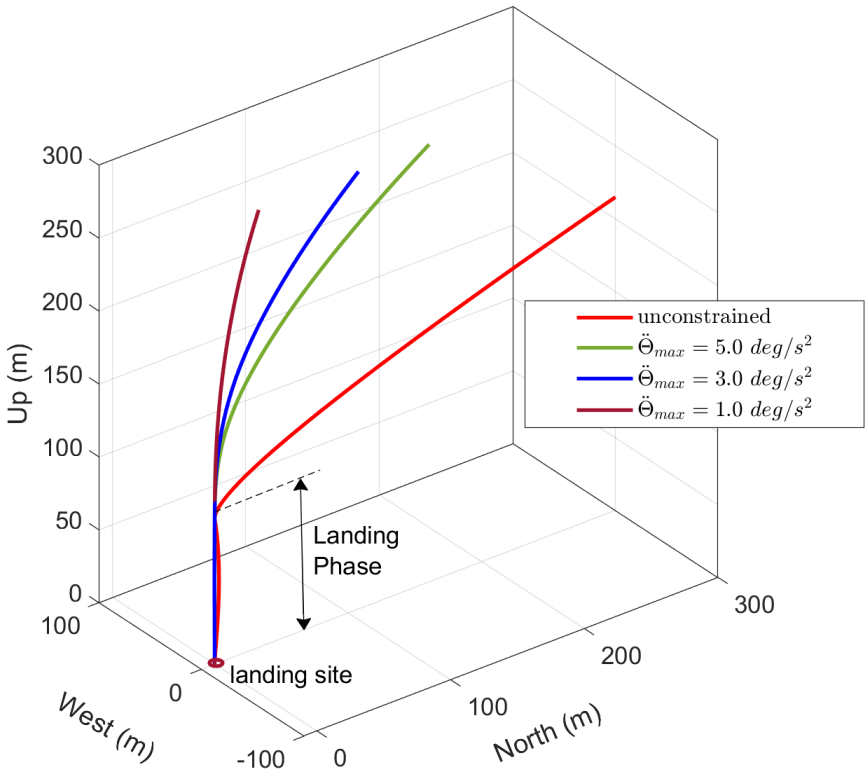

Fig. 9 Descent trajectories near the landing site with Descent Phase guided by G-POLAR and Landing Phase guided by E-Guidance law

of extra burn time. To put this propellant saving in another perspective, the usable amounts of propellant left at LM engine cut-off in all the 6 Apollo lunar landing missions range from 285 kg (628 lb for Apollo 14) to 556 kg (1,225 lb for Apollo 17) [2]. In other words, a crewed lunar landing mission could "earn" the propellant margin equal to the largest in all six Apollo landings just by flying propellant-optimal guidance.

Table 5 Propellant consumption with Descent and Landing Phases (ALDG=Apollo Lunar Descent Guidance)

Guidance	Prop in Descent Phase (kg)	Prop in Landing Phase (kg)	Total prop usage (kg)
G-POLAR + E-Guidance	6,721	86	6,806
ALDG + E-Guidance	7,314	86	7,400

The pointing angle and velocity profiles along the descent trajectory guided by G-POLAR in the Descent Phase and E-Guidance in the Landing Phase are shown in Figs. 12 and 13. The inserts in these figures also depict zoom-in view of the variations during the Landing Phase which lasts about 30 seconds. The pointing constraint drives The pointing angle to zero at the end of the Descent Phase and it remains zero during the Landing Phase for a vertical descent. The velocity in the Landing Phase decreases at a much slower rate from 5 m/s to the specified 1 m/s at touchdown.

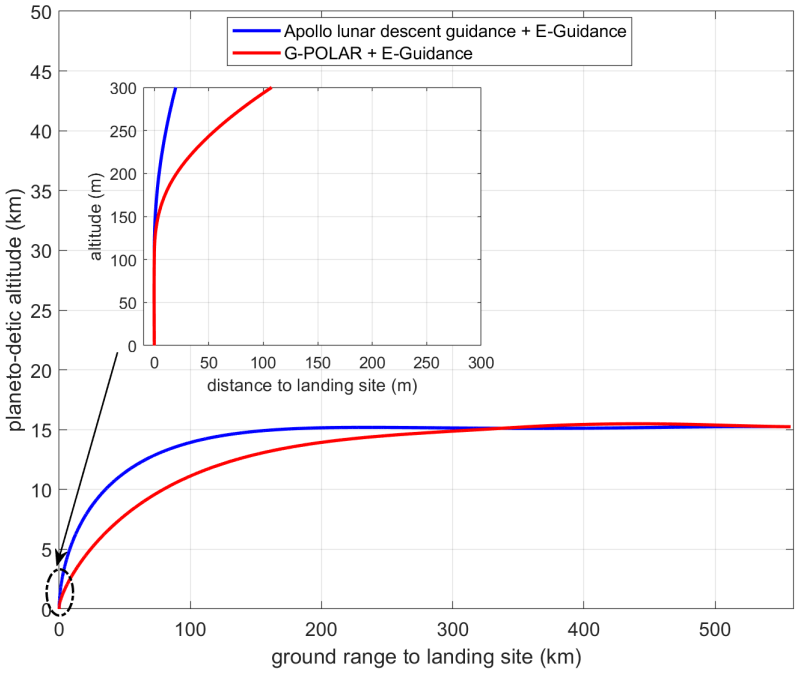

Fig. 10 Descent trajectories guided by G-POLAR plus E-Guidance, and by Apollo lunar descent guidance plus E-Guidance

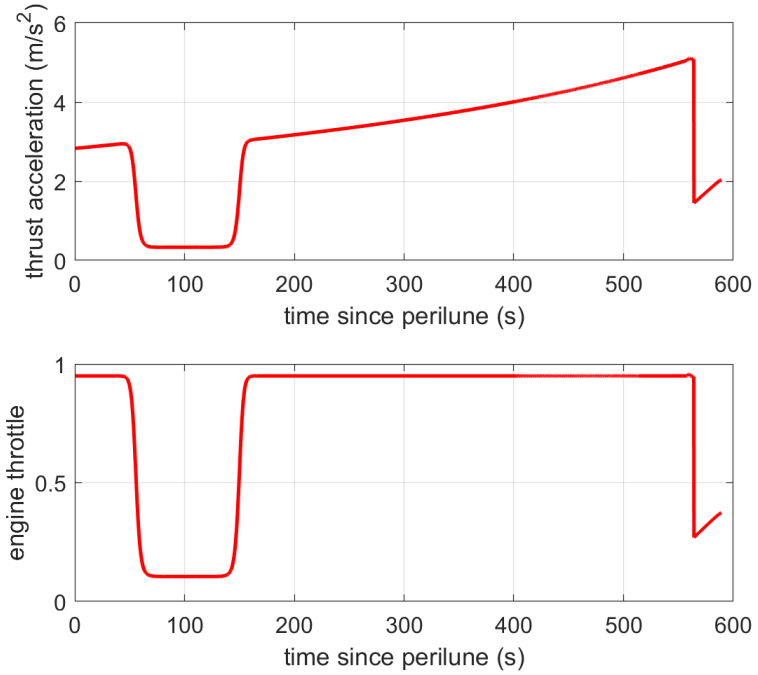

Fig. 11 Throttle profile with Descent Phase guided by G-POLAR and Landing Phase by E-Guidance law

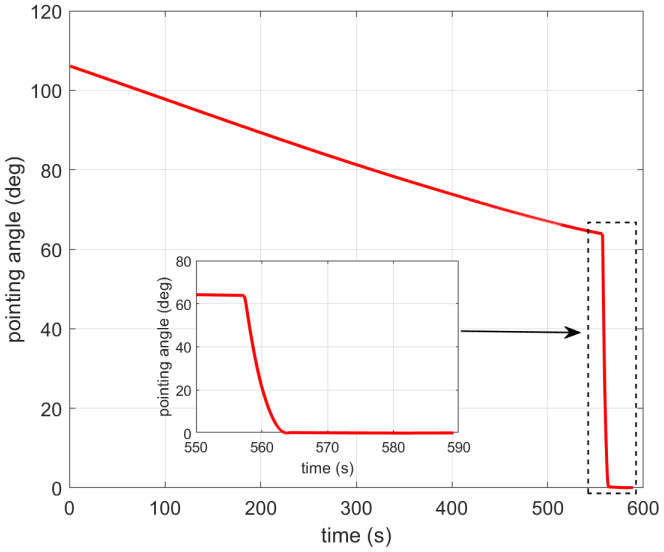

Fig. 12 Pointing-angle profile with Descent Phase guided by G-POLAR and Landing Phase by E-Guidance law

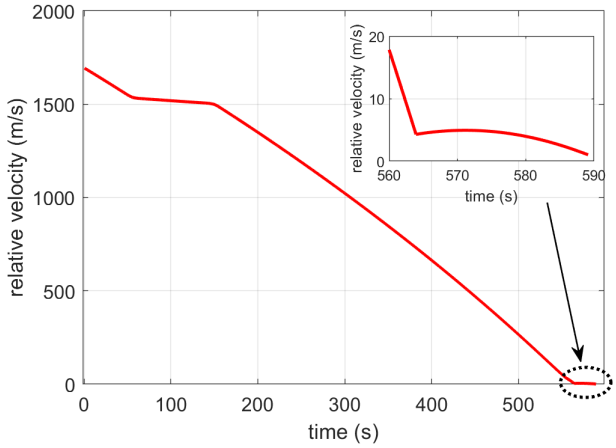

Fig. 13 Velocity profile with Descent Phase guided by G-POLAR and Landing Phase by E-Guidance law

E. Evaluation of Guidance Robustness

To assess the robustness of the guidance strategy with G-POLAR in the Descent Phase and E-Guidance in the Landing Phase, closed-loop Monte Carlo simulations are performed, with dispersions in the PDI condition and uncertainty in a most critical system parameter, the thrust magnitude of the engine of the lander. All the random dispersions and uncertainties are modeled by zero-mean Gaussian distributions. Table 6 gives the 3-σ values of the distributions. The dispersions in the vehicle motion states are assumed to be known to the navigation system (thus known to the guidance system). But the dispersions in the vehicle initial mass and thrust are considered uncertainties and unknown to the guidance system. At full throttle a 2% thrust variation as indicated in Table 6 would be 900 N, greater than the largest difference of 711 N between the predicted and actual thrust observed in the Apollo 11 mission [19].

The statistics of the touchdown conditions of 1000 Monte Carlo closed-loop simulations are summarized in Table 7. The high landing accuracy in terms of the miss distance and touchdown velocity in Table 7 is typical of E-Guidance or Apollo lunar descent guidance law in 3DOF simulation with perfect navigation, especially in vertical or nearly vertical descent. The combined total propellant consumption has a mean of 6,806 kg, exactly the same as the nominal total

Table 6 Dispersions in PDI condition and thrust

Parameter	3-σ Value
Altitude	200.0 (m)
Longitude	0.25 (deg)
Latitude	0.25 (deg)
Inertial velocity	3.3 (m/s)
Inertial flight path angle	0.1 (deg)
Inertial azimuth angle	0.2 (deg)
Total vehicle mass	100.0 (kg)
Engine thrust	2.0%

propellant consumption in Table 5, and a small standard deviation of 15.1 kg, with the maximum at 6,861 kg and minimum at 6,758 kg. The final pointing angle is practically 90 deg in all the cases. And the powered descent averages 600 seconds, with ±5 seconds at the edge of the spread.

Table 7 Statistics of touchdown conditions for 1000 Monte Carlo simulations, guided by optimal bang-bang solution for the descent phase and E-Guidance for the landing phase, subject to the pointing constraint with $\ddot{\Theta}_{max}$ = 3.0 deg/s

	mean	standard deviation	maximum	minimum
miss (m)	3.89-05	1.23E-05	5.95E-05	7.45E-07
descending rate (m/s)	1.11E+00	1.70E-02	1.19E+00	9.57E-01
propellant usage (kg)	6.806E+03	1.506E+01	6.861E+03	6.758E+03
final pointing angle (deg)	8.0E-02	1.3E-02	1.2E-01	4.0E-02
powered descent flight time (s)	5.796E+02	1.694E+00	5.846E+02	5.745E+02

The same 1000 Monte Carlo cases are then rerun, this time with the powered descent phase guided by the optimal constant-throttle guidance by G-POLAR+, and with the same pointing constraint and E-Guidance for the landing phase. The statistics of the touchdown conditions are given in Table 8. The mean propellant consumption is 6,889 kg, only 83 kg more than that under the optimal bang-bang guidance in Table. 7. With the exception of the powered descent flight time, other statistics in Table 8 are very similar to those in Table 7. The powered descent flight time under the constant-throttle guidance is on average 26.4 seconds longer than that under the bang-bang guidance.

Given the ultra simplicity of just requiring the engine to operate at a constant-thrust (NOT constant acceleration) level, and the very close propellant performance, the optimal constant-throttle guidance should be more appealing than the bang-bang throttle guidance. There are other advantages of using the optimal constant-throttle guidance. See Ref.![15] for some discussion.

Table 8 Statistics of touchdown conditions for 1000 Monte Carlo simulations, guided by optimal constant-throttle solution for the descent phase and E-Guidance for the landing phase, subject to the pointing constraint with $\ddot{\Theta}_{max}$ = 3.0 deg/s

	mean	standard deviation	maximum	minimum
miss (m)	5.60E-05	8.66E-6	6.32E-05	5.08E-06
descending rate (m/s)	1.02E+00	2.31E-02	1.09E+00	9.43E-01
propellant usage (kg)	6.889E+03	1.50E+01	6.960E+03	6.853E+03
final pointing angle (deg)	4.0E-02	9.9E-03	6.0E-02	0.0E0
powered descent flight time (s)	6.266E+02	4.315E+00	6.386E+02	6.132E+02

VII. Conclusions

For all the strong research and development activities in recent years in propellant-optimal powered descent guidance, little has been quantitatively known about how much propellant advantage modern optimal guidance could offer over the legacy technology for crewed lunar landings. This work provides such a needed assessment using two recently developed propellant-optimal guidance algorithms, and the venerable Apollo lunar descent guidance law under identical conditions. The assessment has determined that the propellant saving by propellant-optimal guidance is in the range of 7%-9%, in a mission similar to Apollo 11 but landing at the South Pole of the Moon. To put it in a different perspective, employing propellant-optimal guidance would give an identical lander in the same mission two extra minutes of burn time in the final hovering over the landing site. While this study focuses on propellant performance of optimal guidance, there are other potential and consequential advantages of advanced guidance approaches such effective enforcement of trajectory constraints, autonomous divert and hazard avoidance. The legacy powered descent guidance laws, on the other hand, are highly robust and flight proven. It is demonstrated in this paper that modern and legacy powered descent guidance methods may be combined in a crewed lunar mission to reap the strengths of both. This study and the findings may offer a valuable reference and serve to promote more in-depth examinations of propellant-optimal powered descent guidance as a crewed lunar mission begins in earnest.

Acknowledgment

Partial support to this work by the NASA Cooperative Agreement 80NSSC21M0342 is gratefully acknowledged.

References

[1] "Apollo 11 Mission Report," Tech. Rep. NASA SP-238, NASA, 1971.

[2] Orloff, R. W., "Apollo by the Numbers: A Statistical Reference," Tech. Rep. NASA SP-2000-4209, NASA, October 2000.

[3] Acikmese, B., and Ploen, S. R., "Convex Programming Approach to Powered Descent Guidance for Mars Landing," *Journal of Guidance, Control, and Dynamics*, Vol. 30, No. 5, 2007, pp. 1353–1366. doi:10.2514/1.27553.

[4] Blackmore, L., Acikmese, B., and Scharf, D. P., "Minimum Landing Error Powered Descent Guidance for Mars Landing Using Convex Optimization," *Journal of Guidance, Control, and Dynamics*, Vol. 33, No. 4, 2010, pp. 1161–1171. doi:10.2514/1.47202.

[5] Acikmese, B., Carson, J., and Blackmore, L., "Lossless Convexification of Nonconvex Control Bound and Pointing Constraints of the Soft Landing Optimal Control Problem," *IEEE Transactions on Control Systems Technology*, Vol. 21, No. 6, 2013, pp. 2104–2113. doi:10.1109/TCST.2012.2237346.

[6] Dueri, D., Acikmese, B., Scharf, D., and Harris, M., "Customized Real-Time Interior-Point Methods for Onboard Powered-Descent Guidance," *Journal of Guidance, Control, and Dynamics*, Vol. 40, No. 2, 2017, pp. 197–212. doi:10.2514/1.G001480.

[7] Sagliano, M., "Pseudospectral Convex Optimization for Powered Descent and Landing," *Journal of Guidance, Control, and Dynamics*, Vol. 41, No. 2, 2018, pp. 320–334. doi:10.2514/1.g002818.

[8] Szmuk, M., Reynolds, T. P., and Acikmese, B., "Successive Convexification for Real-Time 6-DoF Powered Descent Guidance with State-Triggered Constraints," *Journal of Guidance, Control, and Dynamics*, Vol. 43, No. 8, 2020, pp. 1399–1413. doi:10.2514/1.G004549.

[9] Lu, P., "Propellant-Optimal Powered Descent Guidance," *Journal of Guidance, Control, and Dynamics*, Vol. 41, No. 4, 2018, pp. 813–826. doi:10.2514/1.G003243.

[10] Ito, T., and Sakai, S., "Throttled Explicit Guidance to Realize Pinpoint Landing Under a Bounded Thrust Magnitude," *Journal of Guidance, Control, and Dynamics*, Vol. 44, No. 4, 2021, pp. 854–861. doi:10.2514/1.G005577.

[11] You, S., Dai, R., and Rea, J., "Theoretical Analysis of Fuel-OptimalPowered Descent Problem with State Constraints," *Journal of Guidance, Control, and Dynamics*, Vol. 45, No. 12, 2022, pp. 2350–2359. doi:10.2514/1.G006815.

[12] Leparoux1, C., Hérissé1, B., and Jean2, F., "Optimal Planetary Landing with Pointing and Glide-slope Constraints," IEEE 61st Conference on Decision and Control, 2022, pp. 4357–4362. doi:10.1109/CDC51059.2022.9992735.

[13] Lu, P., and Callan, R., "Propellant-Optimal Powered Descent Guidance Revisited," *Journal of Guidance, Control, and Dynamics*, Vol. 46, No. 2, 2023, pp. 215–230. doi:10.2514/1.G007214.

[14] Ito, T., and Sakai, S., "Optimal Powered Descent Guidance Under Thrust Pointing Constraint," *Journal of Guidance, Control, and Dynamics*, Vol. 46, No. 4, 2023, pp. 695–708. doi:10.2514/1.G006727.

[15] Lu, P., and Davami, C., "Rethinking Propellant-Optimal Powered Descent Guidance," *Journal of Guidance, Control, and Dynamics*, Vol. 47, No. 10, 2024, pp. 2016–2028. doi:10.2514/1.G008343.

[16] Rea, J. R., "An Investigation of Fuel Optimal Terminal Descent," Phd thesis, The University of Texas at Austin, May 2009.

[17] Lee, A. Y., "Fuel-efficient Descent and Landing Guidance Logic for a Safe Lunar Touchdown," AIAA 2011-6499, 2011. doi:10.2514/6.2011-6499.

[18] Klumpp, A. R., "Apollo Lunar Descent Guidance," *Automatica*, Vol. 10, No. 2, 1974, pp. 133–146. doi:10.1016/0005-1098(74)90019-3.

[19] Bennett, F. V., "Apollo Experience Report – Mission Planning for Lunar Module Descent and Ascent," NASA TN D-6846, 1972.

[20] Cherry, G. W., "A General, Explicit, Optimizing Guidance Law for Rocket-Propelled Spaceflight," AIAA Paper 64-638, 1964. doi:10.2514/6.1964-638.

[21] Bennett, F. V., "Apollo Lunar Descent and Ascent Trajectories," NASA TM X-58040, 1970.

[22] Bellman, R., *Dynamic Programming*, 1st ed., Princeton University Press, Princeton, NJ, USA, 1957.

[23] Berning, A. W., Strohl, L. D., and Bieniawski, S., "Lossless Convex Guidance for Lunar Powered Descent," AIAA 2023-2004, 2023. doi:10.2514/6.2023-2004.

[24] Pontryagin, L. S., Boltyanskii, V. G., Gramkreledze, Q. V., and Mishchenko, E. F., *The Mathematical Theory of Optimal Processes*, Intersciences, New York, 1962, Chap. 2.

[25] D'Souza, C. S., "An Optimal Guidance Law for Planetary Landing," AIAA Paper 97-3709, 1997. doi:10.2514/6.1997-3709.

[26] Lu, P., "Theory of Fractional-Polynomial Powered Descent Guidance," *Journal of Guidance, Control, and Dynamics*, Vol. 43, No. 3, 2020, pp. 398–409. doi:10.2514/1.G004556.

[27] Lu, P., "Augmented Apollo Powered Descent Guidance," *Journal of Guidance, Control, and Dynamics*, Vol. 42, No. 3, 2019, pp. 447–457. doi:10.2514/1.G004048.

[28] Sandoval, S. A., and Lu, P., "Powered Descent Guidance for a Crewed Lunar Landing Mission," *AAS Guidance and Control Conference, Breckenridge, CO*, AAS Paper 20–044, 2020.

[29] NASA, "Apollo 11 Lunar Module / EASEP," `https://nssdc.gsfc.nasa.gov/nmc/spacecraft/display.action?id=1969-059C`, . Accessed: 2023-12-28.

[30] S. A. Loff, "Apollo 11 Mission Overview," `https://www.nasa.gov/history/apollo-11-mission-overview/`, . Accessed: 2023-12-28.

[31] Ross, I. M., "Enhancements to the DIDO Optimal Control Toolbox," , 2020. doi:10.48550/ARXIV.2004.13112, URL `https://arxiv.org/abs/2004.13112`.